Quantum Phase Transitions and Continuous Observation of Spinor Dynamics in an Antiferromagnetic Condensate

Y. Liu,[1,*] S. Jung,[1] S. E. Maxwell,[1] L. D. Turner,[2] E. Tiesinga,[1] and P. D. Lett[1,†]

[1]*Joint Quantum Institute, National Institute of Standards and Technology and University of Maryland, Gaithersburg, Maryland 20899, USA*

[2]*School of Physics, Monash University, Victoria 3800, Australia*

(Received 21 November 2008; revised manuscript received 26 January 2009; published 23 March 2009)

Condensates of spin-1 sodium display rich spin dynamics due to the antiferromagnetic nature of the interactions in this system. We use Faraday rotation spectroscopy to make a continuous and minimally destructive measurement of the dynamics over multiple spin oscillations on a single evolving condensate. This method provides a sharp signature to locate a magnetically tuned separatrix in phase space which depends on the net magnetization. We also observe a phase transition from a two- to a three-component condensate at a low but finite temperature using a Stern-Gerlach imaging technique. This transition should be preserved as a zero-temperature quantum phase transition.

DOI: 10.1103/PhysRevLett.102.125301 PACS numbers: 67.85.−d, 03.75.Kk, 03.75.Mn, 64.70.Tg

The study of multicomponent Bose-condensed (superfluid) systems began with ^{4}He-^{6}He mixtures in the 1950s [1] and continued with a two-component ^{87}Rb Bose-Einstein condensate (BEC), with atoms in two different hyperfine states, in the late 1990s [2]. Recent studies have focused on the investigation of spinor condensates where interconversion among multiple spin states leads to spin population dynamics. A number of investigations of this effect, as well as spatial domain formation in both ferromagnetic $F = 1$ ^{87}Rb BECs [3–5] and antiferromagnetic $F = 1$ ^{23}Na BECs [6–8], have been published. The $F = 2$ ^{87}Rb spinor condensate presents ferromagnetic, antiferromagnetic, and cyclic phases [9–12]. In each of these cases, the experimental system can be modeled with a small number of variables.

While the ferromagnetic Rb system is becoming well studied, the antiferromagnetic Na system remains relatively unexplored. The theoretical description of such a system suggests the possibility of manipulating the phase space topology and dynamics of the system in ways not possible in the ferromagnetic system (e.g., altering the separatrix position in phase space with the magnetization of the system) as well as the possibility of observing a quantum-fluctuation-driven phase transition that does not exist in the ferromagnetic system [5,13].

We consider a spinor BEC with spin angular momentum $F = 1$ in the presence of a magnetic field of strength B along the z axis with the populations initialized to a nonequilibrium state. Collisional interconversion between two $m_F = 0$ atoms and one $m_F = +1$ and one $m_F = -1$ atom takes place in the condensate, leading to oscillations in the spin populations. At ultracold temperatures, the collisions between alkali metal atoms conserve the summed spin angular momentum $\vec{f} = \vec{F}_a + \vec{F}_b$. Our system, ^{23}Na, is antiferromagnetic inasmuch as the interaction energy of $f = 2$ collisions is larger than that of $f = 0$ collisions, which indicates that the coupling favors the $m_F = \pm 1$ states over the $m_F = 0$ state.

The linear Zeeman shift induced by the magnetic field does not affect the collisional interconversion, as the magnetic energies before and after the collision are equal in this approximation. The population dynamics are instead driven by an interplay between the quadratic Zeeman shift and the spin-dependent interaction characterized by the difference in the $f = 0$ and $f = 2$ interaction energies. In ^{23}Na, a divergence in the spin oscillation period occurs near a critical magnetic field B_c [5,8,12]. A dependence of B_c on magnetization m (the difference in fractional population ρ_{m_F} between $m_F = +1$ and $m_F = -1$) is predicted in an antiferromagnetic system [5] or in a ferromagnetic system with a radio-frequency (rf) dressing field [14] but has not been previously observed.

We use two complementary methods to observe the spin dynamics in two different time regimes. A Stern-Gerlach separation followed by absorption imaging (SG-AI) directly measures the populations of different spin states and determines the magnetization m. This technique is completely destructive, and only minimal phase information can be inferred from modeling the data. The second method is Faraday rotation spectroscopy which measures the rotation of the polarization of a laser beam. This rotation is proportional to the projection of the atomic spin $\vec{F}$ along the laser propagation direction. It can be used to continuously infer both phase and population information of the spin dynamics over multiple spin oscillations. Other methods of measuring the condensate phase can be found in Ref. [15].

It is hard to determine B_c from just the spin oscillation period; however, we observe a sharp signature to distinguish two characteristic time evolutions in the vicinity of B_c with Faraday rotation spectroscopy. At long times when the oscillations have damped out [8], we use SG-AI to

characterize the mean-field ground state populations as a function of B and m to observe a predicted phase transition from a two- to a three-component spinor BEC.

A ^{23}Na magneto-optical trap containing up to 6×10^9 atoms is prepared. A crossed optical dipole trap derived from a multimode laser at 1070 nm is then loaded, followed by evaporation and rethermalization. A weak magnetic field gradient is applied during 6 s forced evaporation to form a fully polarized BEC of 1.5×10^5 atoms in the $|F = 1, m_F = 1\rangle$ state. The final trap frequencies are $\omega_{x,y,z} \approx (2\pi)220(\sqrt{2}, 1, 1)$ Hz, and the mean Thomas-Fermi radius is 7.2 μm. We ramp up the magnetic field along the z axis while turning off the field gradient. The final value of B ranges between 6.3 and 60.7 μT with an uncertainty of 0.04 μT (all quoted uncertainties are estimated 1 standard deviation, combined statistical and systematic). We can prepare an initial state with any desired m and ρ_0 by an rf pulse to rotate the atomic spin followed by selective removal of atoms in a given m_F state. The rf pulse is resonant with the linear Zeeman splitting, and its amplitude and duration control the superposition of the m_F levels. The removal is performed by a microwave pulse to selectively transfer $|F = 1, m_F\rangle$ atoms to the $F = 2$ state, followed by a laser pulse resonant with these atoms.

The Faraday detection beam is directed along the x axis and red-detuned 225 GHz from the 10 MHz wide $D2$ line of ^{23}Na. The beam is linearly polarized, has a $1/e^2$ waist of 1 mm at the condensate, and has a power of ≈ 50 mW. The setup for Faraday spectroscopy is similar to that outlined in Refs. [16,17]. A carefully chosen aperture is inserted into the imaging plane for an optimal signal-to-noise ratio (SNR), and the Faraday rotation of the linear polarization is detected using a Wollaston prism and an autobalanced differential photodetector (PD) [18]. The Faraday rotation angle oscillates at the Larmor precession frequency f_L. Changes of spin populations and phases are detected as a modulation of the amplitude of the Faraday signal. Our Faraday signal is the short-time power spectral density of the PD output integrated over a narrow bandwidth of 1 kHz around f_L. This is proportional to the slowly varying envelope of $\langle F_x \rangle^2$. A typical example is shown in Fig. 1. We divide the signal into 1 ms time bins, longer than the transform limit of the digital filter (0.16 ms) but short enough to resolve spin oscillations. Over a 100 ms measurement, we thus make 100 distinct measurements of both the spin projection amplitude and f_L, on a single evolving spinor BEC.

The parameters of the Faraday beam are chosen to minimize atom loss from the off-resonant light scattering while maintaining a good single-shot signal. The measured lifetime of the BEC in the presence of the Faraday beam is 100 ms, consistent with the decay of $\langle F_x \rangle$ inferred from Fig. 1 and with the predicted photon scattering time. The dephasing time due to the tensor light shift [19] is 1 order of magnitude longer. The scattering loss is larger than any other backaction in the present experiments. In the absence of the Faraday beam, we observe an energy dissipation which depends on B and the mean particle density $\langle n \rangle$. Under the conditions of Fig. 1(a), the time scale of this dissipation is 5 times longer than the decay seen in this figure, while at high fields [Fig. 1(b)], it becomes comparable. This dissipation is not well understood.

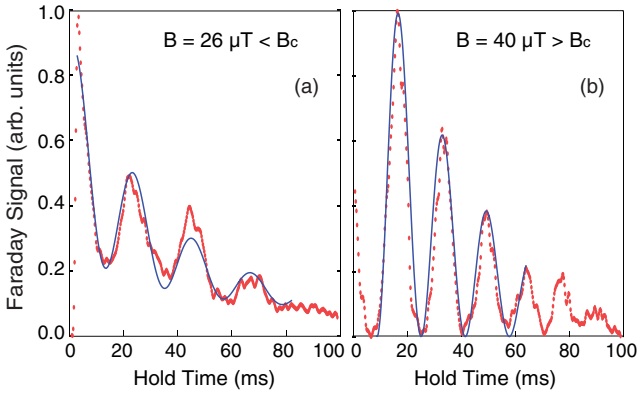

FIG. 1 (color online). Faraday signal (proportional to $\langle F_x \rangle^2$) taken from a single measurement for $m = 0$ at two magnetic fields 26 and 40 μT starting with $\rho_0 = 0.5$, $\theta = 0$. The solid line is a fit with a damped sinusoid. The signals show (a) an oscillating phase and (b) a running phase at B below and above B_c, respectively, as evidenced by the signal reaching zero or not.

Our measurement SNR is limited by the number of atoms in the BEC and the efficiency of the detection [16]. Our BECs are not much larger than needed to get a good single-shot signal with our system. Our detection efficiency could be improved by a factor of 2.

The single mode approximation (SMA) [5,8] is applied to understand our data. The spatial wave function of the BEC is treated as a single mode, and the unit-normalized total wave function can be represented as $\Psi(\mathbf{r}, t) = \Phi(\mathbf{r}) \times [\sqrt{\rho_{-1}(t)}e^{i\theta_{-1}(t)}, \sqrt{\rho_0(t)}e^{i\theta_0(t)}, \sqrt{\rho_{+1}(t)}e^{i\theta_{+1}(t)}]$, where ρ_{m_F} and phases θ_{m_F} are independent of position. The Hamiltonian conserves the particle number and m. The system is described using ρ_0 and $\theta = \theta_{-1} + \theta_{+1} - 2\theta_0$, with the conserved classical spinor energy

$$E = E_{\mathrm{qz}}(1 - \rho_0) + c\rho_0[(1 - \rho_0) + \sqrt{(1 - \rho_0)^2 - m^2}\cos\theta]. \quad (1)$$

Here E_{qz} is the quadratic Zeeman shift $[E_{\mathrm{qz}}/h = (0.0277\ \mathrm{Hz}/(\mu\mathrm{T})^2)B^2]$, $c = c_2\langle n \rangle$ is the spin-dependent collision energy, and c_2 is 1.59×10^{-52} J m^3 for ^{23}Na [8]. The evolution of ρ_0 and θ is given by $\dot{\rho}_0 = -(2/\hbar)\partial E/\partial\theta$ and $\dot{\theta} = (2/\hbar)\partial E/\partial\rho_0$, respectively.

Figure 2 shows typical phase diagrams of the equal-energy contours of Eq. (1) for $m = 0$ at two magnetic fields. The preparation of the state determines the energy $E_0(B)$. Our initial states have $\theta = 0$. At any magnetic field, we can define a separatrix, i.e., that energy contour $E_{\mathrm{sep}}(B)$,

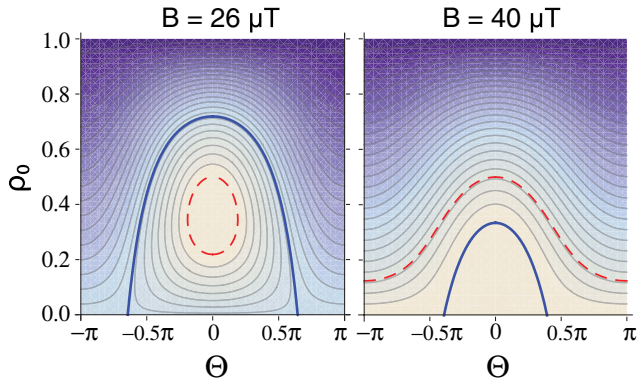

FIG. 2 (color online). Equal-energy contour plots generated from Eq. (1) at two magnetic fields 26 (left) and 40 μT (right), with $m = 0$ and $c/h = 33$ Hz. Dashed (red) lines represent the energy of a state with $\rho_0(t = 0) = 0.5$. Heavy (blue) solid lines represent the energy of the separatrix (E_{sep}) between oscillating and running phase solutions. Darker colors represent lower energies.

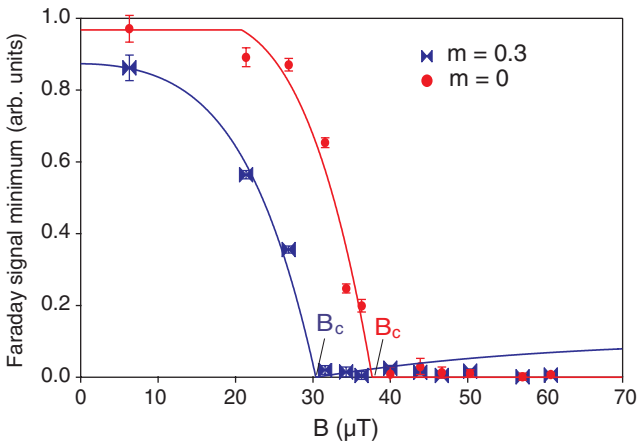

FIG. 3 (color online). The minimum of the Faraday signal as a function of magnetic field for $m = 0$ (red dots) and $m = 0.3$ (blue bowties). A scale factor is applied to the Faraday signal to correct for the PD response at different f_L. The lines are fits based on Eq. (2), which yield the fit parameters $\rho_0 = 0.42$ and $N = 1.50 \times 10^5$ for $m = 0$ and $\rho_0 = 0.54$ and $N = 1.32 \times 10^5$ for $m = 0.3$. The fit parameters are within the 3% uncertainty of those derived from absorption images.

on which there is a saddle point where $\dot{\rho}_0 = \dot{\theta} = 0$. This defines the boundary between two regions in phase space. In fact, $E_{\mathrm{sep}}(B) = E_{\mathrm{qz}}$ in our system.

When $E_0(B) > E_{\mathrm{sep}}(B)$, the value of θ is restricted, while for $E_0(B) < E_{\mathrm{sep}}(B)$ there is no bound. This defines regions with an oscillating phase and a running phase, respectively. In both regions, ρ_0 oscillates. At $E_0(B) \gg E_{\mathrm{sep}}$, which corresponds to small magnetic fields, the period only weakly depends on the field. In the opposite limit, the period decreases rapidly with increasing field. When $B \approx B_c$, defined by $E_0(B_c) = E_{\mathrm{sep}}(B_c)$, the oscillation becomes anharmonic and the period diverges for $B = B_c$.

In the SMA, the Faraday signal is derived from

$$\langle F_x \rangle = \cos\left[\frac{\theta + (\theta_{+1} - \theta_{-1})}{2}\right]\sqrt{\rho_0(1 + m - \rho_0)} + \cos\left[\frac{\theta - (\theta_{+1} - \theta_{-1})}{2}\right]\sqrt{\rho_0(1 - m - \rho_0)}. \quad (2)$$

The phase difference $\theta_{+1} - \theta_{-1}$ is determined by the fast Larmor precession and a slow evolution due to ρ_0 and θ [5]. For $m = 0$, our Faraday signal is proportional to $\rho_0(1 - \rho_0)\cos^2(\theta/2)$. For oscillating phase solutions, θ oscillates about zero (with amplitude $< \pi$), and thus the signal is always greater than zero. On the other hand, the signal is periodically zero for running phase solutions. Figure 1 shows signals from the two regions. For $m \neq 0$, the signal is described by a more complicated expression, but the distinction between the two regions in the vicinity of B_c remains the same.

This provides a sharp signature for locating B_c. Figure 3 shows the value of the minimum of the Faraday signal at different B and m after removal of the exponential decay. For the two magnetizations, a transition from an oscillating phase solution to a running phase solution provides the sharp signature to locate B_c. In Ref. [8], the population oscillations were measured using SG-AI and fit by a sinusoid to extract a period and to locate the two regions of phase space. No sharp experimental signature distinguishing the boundary was observed.

Figure 3 also shows a comparison between the prediction from the SMA and the data. For $m = 0$, the agreement is excellent. For $m = 0.3$, however, the prediction does not agree with our measurements for fields significantly larger than B_c. At the transition point, the minimum of the Faraday signal goes to zero, but above this point, the theory predicts that the minimum rises with B, even though the solution has a running phase. This increase is not observed. The apparent agreement between the SMA theory and our measurements has been surprising—at every magnetic field reported in this Letter, we have seen the presence of several spatial modes or spin domains during the spin oscillations, although not in steady state. The observation of spin domains is in marked contrast to our previous work [8]. Several technical changes may have contributed to the domain formation, such as a 50% increase of the total atom number and more stable magnetic fields. Understanding how multiple spatial modes affect the spin dynamics is an interesting direction for future research.

At long times, after the oscillations have damped out, we can study the mean-field ground state of this system. Within the SMA, a quantum phase transition from a three- to a two-component BEC is predicted for the mean-field ground state [13]. We use SG-AI as a direct way to measure the equilibrium populations and to observe this phase transition.

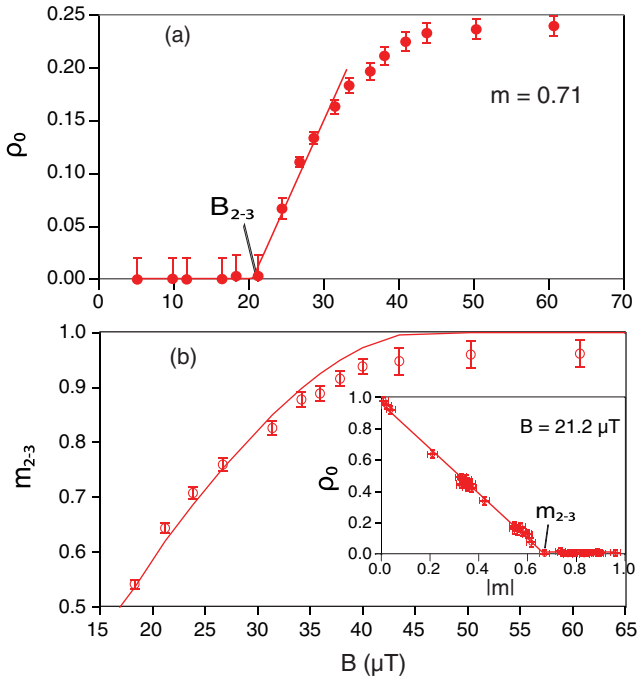

FIG. 4 (color online). Evidence of phase transitions in the mean-field ground state of the antiferromagnetic spinor BEC. (a) Points indicate ρ_0 as a function of B at $m = 0.71(2)$. The intersection of two linear fits defines B_{2-3}, the critical magnetic field for the phase transition. (b) Inset: ρ_0 versus m for $B = 21.2$ μT. The intersection of two linear fits defines m_{2-3}, the critical magnetization. The main figure shows m_{2-3} versus B. The solid line is the prediction from the SMA.

The behavior of the variance of ρ_0 allows us to determine when the system reaches a steady state. At a given time, we measure ρ_0 25–30 times and calculate a variance. In the steady state, the variance reaches a minimum. Because of technical noise in atom counting, this variance is larger than that predicted by a quantum calculation of the spinor ground state [20]. We find that a steady state for $m = 0$ is reached within our maximum hold time of 10 s for $B \geq 18$ μT. For nonzero m, the steady state is reached much faster.

Figure 4(a) shows the steady-state values of ρ_0 as a function of B. For each measurement, we prepare nearly identical initial states at $B = 24.4$ μT to set the populations and magnetizations. We then wait 4 s to reach the steady state before adiabatically ramping the field to a desired final value over 500 ms. We then wait another 5 s before making an SG-AI measurement. In the inset in Fig. 4(b), however, each initial state is directly prepared with a different magnetization. In both figures, a transition between a two-component BEC with $\rho_0 = 0$ and a three-component BEC with nonzero ρ_0 is observed. A critical magnetic field B_{2-3} and a critical magnetization m_{2-3} are defined and extracted from the intersection of two linear fits to the data. Good agreement is found between the experimental value of m_{2-3} and the prediction from the SMA [13], as shown in Fig. 4(b). This confirms a phase transition from a three- to a two-component spinor BEC in the antiferromagnetic mean-field ground state. Although it is observed here at a finite temperature, the phase transition should remain at zero temperature, where the transition would be driven solely by quantum fluctuations. It has been predicted that this phase transition persists even when the spin states do not share the same spatial distribution and the SMA is no longer appropriate [13].

In conclusion, we have demonstrated that Faraday rotation spectroscopy provides a method to continuously monitor the spin dynamics in a spinor BEC. The technique provides a sharp signature to locate the boundary in phase space between the oscillating and running phase solutions. We observe a dependence of the position of this separatrix on the magnetization. In addition, we have confirmed a quantum phase transition from a two- to a three-component BEC in the mean-field ground state. Physics beyond the SMA, possibly similar to Landau damping of excitations of a single component BEC [21], may explain the dissipation leading to the equilibrium observed in these experiments.

We thank W. D. Phillips, J. V. Porto, and E. Gomez for insightful discussions and ONR for financial support. S. M. thanks the NIST/NRC postdoctoral program.

*yingmei.liu@nist.gov
†paul.lett@nist.gov

[1] L. Guttman and J. R. Arnold, Phys. Rev. **92**, 547 (1953).
[2] C. J. Myatt *et al.*, Phys. Rev. Lett. **78**, 586 (1997).
[3] M. S. Chang *et al.*, Nature Phys. **1**, 111 (2005).
[4] M. S. Chang *et al.*, Phys. Rev. Lett. **92**, 140403 (2004).
[5] W. Zhang *et al.*, Phys. Rev. A **72**, 013602 (2005).
[6] J. Stenger *et al.*, Nature (London) **396**, 345 (1998).
[7] H. J. Miesner *et al.*, Phys. Rev. Lett. **82**, 2228 (1999).
[8] A. T. Black *et al.*, Phys. Rev. Lett. **99**, 070403 (2007).
[9] A. Widera *et al.*, New J. Phys. **8**, 152 (2006).
[10] T. Kuwamoto *et al.*, Phys. Rev. A **69**, 063604 (2004).
[11] H. Schmaljohann *et al.*, Phys. Rev. Lett. **92**, 040402 (2004).
[12] J. Kronjager *et al.*, Phys. Rev. Lett. **97**, 110404 (2006).
[13] W. Zhang, S. Yi, and L. You, New J. Phys. **5**, 77 (2003).
[14] M. Vengalattore *et al.*, Phys. Rev. Lett. **100**, 170403 (2008).
[15] J. M. Higbie *et al.*, Phys. Rev. Lett. **95**, 050401 (2005); Y. J. Wang *et al.*, Phys. Rev. Lett. **94**, 090405 (2005); M. H. Wheeler *et al.*, Phys. Rev. Lett. **93**, 170402 (2004); M. Saba *et al.*, Science **307**, 1945 (2005).
[16] G. A. Smith, S. Chaudhury, and P. S. Jessen, J. Opt. B **5**, 323 (2003).
[17] M. L. Terraciano *et al.*, Phys. Rev. A **77**, 063417 (2008).
[18] P. C. D. Hobbs, Appl. Opt. **36**, 903 (1997).
[19] G. A. Smith *et al.*, Phys. Rev. Lett. **93**, 163602 (2004).
[20] L. Chang *et al.*, Phys. Rev. Lett. **99**, 080402 (2007).
[21] L. Pitaevskii and S. Stringari, Phys. Lett. A **235**, 398 (1997).